Tuning out vibrational levels in molecular electron energy-loss spectra

A. N. Heays, B. R. Lewis, and S. T. Gibson
Research School of Physics and Engineering, The Australian National University, Canberra, ACT 0200, Australia

C. P. Malone, P. V. Johnson, and I. Kanik
Jet Propulsion Laboratory, California Institute of Technology, 4800 Oak Grove Drive, Pasadena, California 91109, USA

M. A. Khakoo
Department of Physics, California State University, Fullerton, California 92834, USA
(Received 11 December 2011; published 18 January 2012)

The phenomenon whereby features associated with certain vibrational levels in molecular states of mixed electronic character disappear under specific scattering conditions in electron energy-loss spectra is investigated. In particular, using a combination of experimental measurements and coupled-channel calculations, anomalous vibrational intensities in the mixed valence-Rydberg $^1\Pi_u \leftarrow X\,^1\Sigma_g^+$ transition of N_2 are explained. A single parameter, i.e., the ratio of the generalized electronic transition moments to the diabatic valence and Rydberg components of the mixed states, dependent on the experimental scattering conditions, is found to be essentially capable of describing all observed relative vibrational intensities, including the near disappearance of the $b\,^1\Pi_u(v = 5)$ feature for momentum-transfer-squared values $K^2 \approx 0.3$ a.u. This result highlights the interesting possibility of experimental control of molecular quantum-interference effects in electron energy-loss spectra, something that is not possible in optical spectra.

DOI: 10.1103/PhysRevA.85.012705 PACS number(s): 34.80.Gs, 31.50.Gh

I. INTRODUCTION

Non-Franck-Condon vibrational intensity anomalies are widely observed in optical transitions to excited molecular states of mixed electronic character. Essentially, these anomalies are due to quantum-interference effects between the transition amplitudes for the excitation of the contributing electronic basis states. Such interference effects have been discussed at length, e.g., by Lefebvre-Brion and Field [1]. If we consider the specific case of two coupled diabatic-basis electronic states $\hat{1}$ and $\hat{2}$ in a diatomic molecule, then the fundamental quantity controlling the magnitude and sense of the interference effect, and, therefore, the corresponding intensity anomalies in the vibrational structures of each mixed transition from an initial state 0, is [1]

$$M_{\hat{1}0}(R)V_{\hat{1}\hat{2}}(R)M_{\hat{2}0}(R), \tag{1}$$

where the $M_{\hat{i}0}(R)$ are the electronic transition moments, $V_{\hat{1}\hat{2}}(R)$ is the electronic coupling, and R is the internuclear distance. For the case of optical transitions in an isolated molecule, the parameters in (1) are immutable, and the corresponding non-Franck-Condon vibrational intensity behavior is a fixed characteristic of the molecule.

In the case of molecular electronic excitation by electron impact, the optical selection rules are relaxed and transition intensities depend also on the scattering conditions. Traditionally, the relationship between optical and electron energy-loss (EEL) spectra has been considered using the concept of the generalized oscillator strength, introduced by Bethe [2] and usually formulated within the first Born approximation. However, Lassettre *et al.* [3] showed that, even if the first Born approximation does not apply, a generalized oscillator strength can be defined which becomes the optical oscillator strength in the limit of vanishing momentum transfer. Similarly, a generalized electronic transition moment (GETM) can be defined which becomes the electric-dipole transition moment in the same limit. Within the adiabatic-nuclei approximation [4], the fundamental quantity controlling interference effects in EEL spectra accessing two coupled states is analogous to (1), but with the electronic transition moments replaced by the corresponding GETMs, which contain the kinematical effects. The key difference from the optical case is that the relative vibrational intensities in the EEL case are dependent on the scattering conditions. Thus, electron-impact excitation allows the possibility of *experimental control* over the molecular quantum-interference effects.

This phenomenon has received little attention previously. However, in a landmark study, Dillon *et al.* [5] performed *ab initio* generalized oscillator strength calculations within the first Born approximation in order to explain $E\,^3\Sigma_u^- \leftarrow X\,^3\Sigma_g^-$ vibrational intensity anomalies in the EEL spectrum of O_2. Subsequently, Lewis *et al.* [6] applied the concept of the GETM to detailed coupled-channel calculations of the mixed Rydberg-valence $^3\Sigma_u^-$ and $^3\Pi_u$ states of O_2, finding that a single parameter, i.e., the ratio of the diabatic GETMs to the Rydberg and valence components of the mixed states, controlled the evolution of the corresponding EEL vibrational intensity distributions as the scattering conditions were changed. The Rydberg GETMs were found to decrease faster than the valence GETMs as the scattering angle decreased or the impact energy decreased. They [6] also noted that, for some vibrational levels, constructive interference between the Rydberg and valence transition amplitudes produced "persistent lines" under these same higher momentum-transfer conditions, creating the chance for misassignment as forbidden transitions in EEL spectra.

The nitrogen molecule is also expected to be an excellent candidate for the investigation of interference effects in EEL spectra, since its lowest dipole-allowed transitions have been known for many years to be dominated by transitions into

strongly interacting Rydberg and valence states, of both $^1\Pi_u$ and $^1\Sigma_u^+$ symmetry [7–9]. While there have been many experimental studies in the relevant 12–13.8 eV energy-loss region, reviewed by Khakoo *et al.* [10], only one [11] has attempted to quantify interference effects in the vibrational intensities. In that work [11], the vibrational intensity pattern of the mixed Rydberg-valence $b\ ^1\Pi_u$ features in EEL spectra, significantly different from the optical pattern [12], was found to be more consistent with a two-channel picture in which the Rydberg GETM was negligible.

In the precursor [10] to the present study, differential cross sections (DCSs) for the electron-impact excitation of many electronic states of N_2 were deduced from EEL spectra in the 12–13.8 eV energy-loss region, taken at a resolution of ∼40 meV full width at half maximum (FWHM). In this work, we are concerned specifically with examining the evolution, in response to the scattering conditions, of relative vibrational intensities in EEL spectra accessing the mixed Rydberg and valence states of $^1\Pi_u$ symmetry in N_2, with an emphasis on the nominal valence state $b\ ^1\Pi_u$. To that end, the spectra of Ref. [10] are supplemented here by new, higher-resolution EEL measurements, enabling better discrimination of the pertinent individual vibrational features, while a coupled-channel theoretical treatment of the relevant interference effects is employed to explain the evolution of the vibrational intensities.

II. EXPERIMENTAL METHOD

In order to facilitate the comparison with theory, generalized vibrational oscillator strengths (GVOSs) [6] were derived for each feature in the new EEL spectra. The experimental and analytical procedures used to determine the absolute DCSs have been described in detail by Khakoo *et al.* [10]. Here, only a brief description of these procedures is provided, together with a discussion of the derivation of GVOSs and estimated uncertainties from the measured vibrationally resolved DCSs.

Cylindrical electrostatic optics and double hemispherical energy selectors were utilized, both in the electron gun and in the detector [10,13]. The target N_2 beam was formed by effusing the gas through a thin-aperture system [14], with a backing pressure of ∼2 Torr. New energy-loss spectra, including both the elastic peak and the inelastic region from 12.2 to 13.8 eV, were collected at fixed impact energies (E_0 = 30, 50, and 100 eV) and scattering angles ($1^\circ \leqslant \theta \leqslant 90^\circ$) by repetitive, multi-channel-scaling techniques. The composite energy resolution of the scattered electrons was minimized (∼30 meV FWHM) while maintaining reasonable count rates. These requirements, together with the mostly forward-peaked structure of the DCSs, limited the practical scattering angular range to $\theta \leqslant 90^\circ$.

Background subtraction using the movable-source method [15] allowed the determination of the ratios of relative inelastic DCSs of the summed states in the energy-loss region of interest to the relative elastic DCSs. Regions clear of energy-loss features defined the background for the inelastic energy-loss spectra. The summed DCS data were renormalized using the inelastic energy-loss signal of the $n = 2$ states of He [16] to correct for any transmission effects. While the He results of Trajmar *et al.* [16] were utilized in the present work, more recent data show good agreement [17,18]. The measured spectra were unfolded, leaving all vibrational levels of the $a''\ ^1\Sigma_g^+$, $b\ ^1\Pi_u$, $c\ ^1\Pi_u$, $o\ ^1\Pi_u$, $b'\ ^1\Sigma_u^+$, $c'\ ^1\Sigma_u^+$, $D\ ^3\Sigma_u^+$, $G\ ^3\Pi_u$, and $F\ ^3\Pi_u$ states as independent features, rather than using Franck-Condon factors to fix their relative intensities, similar to our approach in a number of recent works [10,19,20]. A nonlinear least-squares algorithm was used to fit the features in each multi-channel spectrum in the energy-loss region of interest, with a line shape determined empirically by the separate fitting of a multi-Gaussian function to the isolated $a''(0)$ feature. A number of vibronic levels could not be resolved experimentally due to their proximity to each other in energy loss (see Table I of Khakoo *et al.* [10]), specifically, $b(4) \sim D(0)$, $b(5) \sim F(0)$, $o(0) \sim D(1)$, $b(9) \sim o(1)$, $c(1) \sim F(1)$, and $b'(8) \sim o(2)$. Nevertheless, in these cases each unresolved level was treated independently in the fitting procedure, with the relevant energy splitting fixed at the optical-spectroscopic value, and the intensities attributed by the fitting algorithm to each level within a given pair summed to give a net signal for the unresolved pair. In the present study, the interpretation of the intensity attributed to the unresolved $b(5) \sim F(0)$ pair is of particular importance. At the impact energies employed, which are well above threshold, the optically allowed $b(5)$-level contribution is expected to dominate (at small θ) that from the forbidden triplet $F(0)$-level excitation, with similar conclusions for the unresolved $b(4) \sim D(0)$, $o(0) \sim D(1)$, and $c(1) \sim F(1)$ features.

Inelastic-to-elastic ratios were obtained for each unfolded inelastic feature by comparing the individual relative intensities of the vibrational features of each electronic state with the summed intensities. This procedure minimizes uncertainties in our analysis involving the spectrometer transmission and results in more accurate relative inelastic DCSs over extended energy-loss ranges. Absolute inelastic DCSs were then obtained by multiplying the inelastic-to-elastic ratios by an average of selected experimental DCSs for elastic electron scattering from N_2 [10]. Although recent elastic DCS measurements by Muse *et al.* [21] and Linert and Zubek [22] are available, which demonstrate good consistency with previous DCSs within the quoted uncertainties (∼10 − 15%), we used the experimental elastic DCSs of Srivastava *et al.* [23] (corrected by Trajmar *et al.* [24]), Shyn and Carignan [25] (corrected by Trajmar *et al.* [24]), Nickel *et al.* [26], and Gote and Ehrhardt [27]. In our selection, we used those values that agreed within their combined quoted uncertainties and chose to use our previously applied set of elastic DCSs to minimize any systematic uncertainty in the normalization method (i.e., our present measurement is on equal footing with our previous measurements as far as elastic scattering normalizations are concerned). Absolute DCSs were converted into GVOSs according to the following relation:

$$\mathrm{GVOS}(K^2) = 0.5\, W K^2 \sqrt{E_0/E_\mathrm{R}}\ \times \mathrm{DCS}, \qquad (2)$$

where the GVOS is dimensionless and all other quantities are in atomic units. In Eq. (2), the energy loss $W = E_0 - E_\mathrm{R}$, where E_R is the residual energy, and the square of the momentum transfer, K^2, is given by

$$K^2 = 4[E_\mathrm{R} + W/2 - \sqrt{E_\mathrm{R}(W + E_\mathrm{R})}\cos\theta]. \qquad (3)$$

Uncertainties in the individual quantities used to determine the K^2 and GVOS values were propagated through the calculation to determine the uncertainties in θ ($\pm 2^\circ$), E_0 (± 50 meV), W (± 2 meV), and the DCSs. In determining the uncertainties in the DCSs, we considered the statistical and fitting uncertainties in the individual scattering intensities (typically 2–25%), the uncertainties in the available elastic-scattering DCSs ($\sim 14\%$), the uncertainty propagated by the present inelastic-to-elastic ratio measurements ($\sim 5\%$), and an additional uncertainty of $\sim 10\%$ for the transmission function.

III. THEORETICAL METHOD

A. Coupled channels

In the case of Rydberg and valence states of the same symmetry with molecular-orbital configurations differing in two of the occupied orbitals, such as the $^1\Pi_u$ and $^1\Sigma_u^+$ states of N_2 in the energy range of interest, there may be strong interactions which invalidate the Born-Oppenheimer approximation for the isolated molecule [1]. Here, we address the breakdown of the Born-Oppenheimer approximation by using a coupled-channel (CC) Schrödinger-equation model in which the interactions between the Born-Oppenheimer basis states are included explicitly. A diabatic basis is employed, i.e., the diabatic Born-Oppenheimer basis-state potential-energy curves cross and interact through off-diagonal elements of the electrostatic Hamiltonian $\mathcal{H}^{\rm el}$. This has the attractive property that the associated wave functions, potential-energy curves, and coupling matrix elements can be expected to change relatively smoothly with R.

The CC formalism, detailed by van Dishoeck *et al.* [28] and Torop *et al.* [29], has been used extensively in studies of diatomic molecular spectroscopy and photodissociation dynamics, in particular for OH [28], CO [30], O_2 [31–34], and N_2 [35–38], including planetary-atmospheric applications [39–44]. In this work, we follow the approach of Lewis *et al.* [6], and extend the application of the CC technique to a description of diatomic-molecular electron-impact excitation, obtaining accurate coupled-channel radial wave functions for the target N_2 molecule, while retaining the adiabatic-nuclei approximation in the description of the electron-scattering process. In this approximation, the evolution of the EEL excitation spectrum from the optical limit as the momentum transfer increases is governed, essentially, only by the relative changes in the GETMs for the transitions into the interacting states.

A detailed description of the CC treatment of electron-impact excitation has been given previously [6]. Briefly, if rotation, fine structure, and degeneracy factors are neglected, the adiabatic-nuclei GVOS density for excitation from an initial (uncoupled) electronic state Φ_0 into the m coupled states $\Phi_n, n = 1,2,\ldots,m$, which include m_o open channels, is given, in matrix form, by

$$\frac{df^{\rm an}_{W,0v''}(E_0,\theta)}{dW} = 2W|\langle \boldsymbol{\chi}_W(R)|\mathbf{M}^{\rm FN}(E_0,\theta;\,R)|\chi_{0v''}(R)\rangle|^2, \tag{4}$$

where $\boldsymbol{\chi}_W(R)$ is the CC diabatic radial wave function matrix, of dimension $m \times m_o$, and $\mathbf{M}^{\rm FN}(E_0,\theta;\,R)$ is the fixed-nuclei GETM vector, of dimension $m \times 1$, with elements given by the diabatic-basis GETMs $M^{\rm FN}_{n0}$. The CC radial wave function matrix $\boldsymbol{\chi}_W(R)$ is the solution of the diabatic-basis CC Schrödinger equations, expressed in matrix form,

$$\left\{\mathbf{I}\frac{d^2}{dR^2} + 2\mu\,[W\mathbf{I} - \mathbf{V}(R)]\right\}\boldsymbol{\chi}_W(R) = \mathbf{0}, \tag{5}$$

where μ is the molecular reduced mass, $\mathbf{I}$ is the identity matrix, and $\mathbf{V}(R)$, of dimension $m \times m$, is the symmetric diabatic potential matrix. The diagonal elements of $\mathbf{V}(R)$ are the diabatic electronic potential-energy curves $V_{nn}(R) = \langle\Phi_n|\mathcal{H}^{\rm el}|\Phi_n\rangle$, and the couplings between the interacting electronic states are given by the off-diagonal elements of $\mathbf{V}(R)$, $V_{nj}(R) = \langle\Phi_n|\mathcal{H}^{\rm el}|\Phi_j\rangle$, $j = 1,2,\ldots,m$. In this work, energy-integrated adiabatic-nuclei GVOS densities calculated using Eq. (4) for relevant vibronic transitions are compared with the corresponding experimental GVOSs determined from the EEL spectra using Eq. (2), thereby using the observed vibrational intensity anomalies to provide information on the evolution of the relative GETMs into the interacting electronic states.

B. The N_2 model

A valuable understanding of the interactions within the dipole-accessible $^1\Pi_u$ and $^1\Sigma_u^+$ manifolds of N_2 has been gained from the pioneering semiempirical CC model of N_2 spectroscopy developed by Stahel *et al.* [45], and the subsequent *ab initio* calculations of Spelsberg and Meyer [46]. More recently, using a semiempirical CC model including spin-orbit interactions with the $^3\Pi_u$ manifold, Lewis *et al.* [35] have succeeded in explaining quantitatively the observed pattern of predissociation in the lower $^1\Pi_u$ levels of N_2, while further models have been developed for the $^3\Pi_u$ [37] and $^3\Sigma_u^+$ [38] states.

Here, we are concerned principally with the $^1\Pi_u$ states and employ the CC model of Ref. [35], which includes the valence state $b\ ^1\Pi_u$, the Rydberg states $3p\pi_u\ c\ ^1\Pi_u$ and $3s\sigma_g\ o\ ^1\Pi_u$, together with the $C\ ^3\Pi_u$ and $C'\ ^3\Pi_u$ states. The corresponding diabatic potential-energy curves are shown in Fig. 1. The mutual electrostatic couplings within the singlet and triplet manifolds, together with the singlet-triplet spin-orbit couplings, which control the singlet predissociation behavior, are taken from Ref. [35]. While the triplet states have no significant impact on the present study which is concerned only with intensities, they provide the only open channel in the energy range of interest and are therefore included simply so that Eq. (4) may be applied.

The CC-model diabatic electronic transition moments, pertinent to the *optical* case, are shown in Fig. 2. These electronic transition moments, optimized by comparison with experimental optical oscillator strengths, as described in Ref. [36], are in reasonably good agreement with the *ab initio* calculations of Spelsberg and Meyer [46]. In this work, it is only these model electronic transition moment parameters which are varied, simply by scaling, in order to best fit the experimental GVOS pattern, yielding GETMs appropriate to the particular scattering conditions.

The case of N_2 is somewhat more complicated than that of O_2 [6] since there are *two* Rydberg series, converging on the ground and first-excited electronic states of the molecular ion,

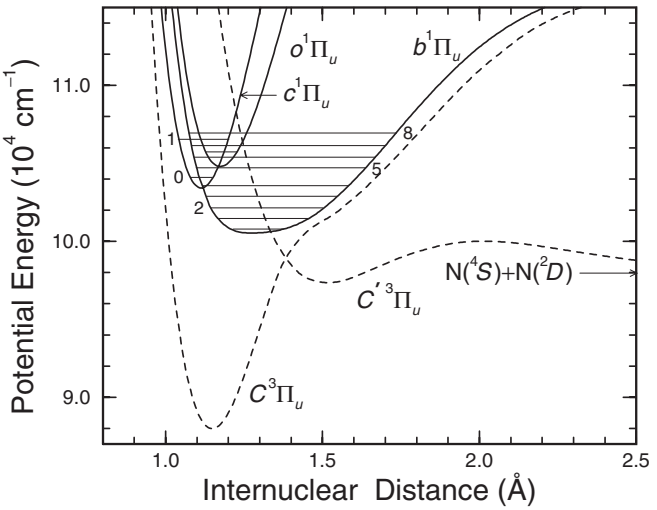

FIG. 1. Diabatic potential-energy curves used in the CC model, referred to the $v = 0, J = 0$ level of the $X\ ^1\Sigma_g^+$ ground state (not shown). Solid curves: $^1\Pi_u$ states. Dashed curves: $^3\Pi_u$ states. The lowest singlet levels are indicated, associated with the nominal diabatic potential-energy curve, and emphasizing the perturbation resulting from the $b \sim c$ crossing.

of which the c and o states are the first members, respectively. Initial attempts to determine three independent GETMs, M_{bX}, M_{cX}, and M_{oX}, for all GVOS data sets failed due to suboptimum signal-to-noise ratios and a comparative lack of sensitivity to M_{oX}. This is not surprising, however, since it is well known [45,46] that V_{bc} is the dominant Rydberg-state–valence-state interaction, with the b- and c-state potential-energy curves crossing near the c-state minimum, as seen in Fig. 1. Therefore, subsequently in the least-squares fitting procedure, the two Rydberg GETMs were taken to behave similarly with respect to the valence GETM as the scattering conditions changed from the optical case. Thus, the main

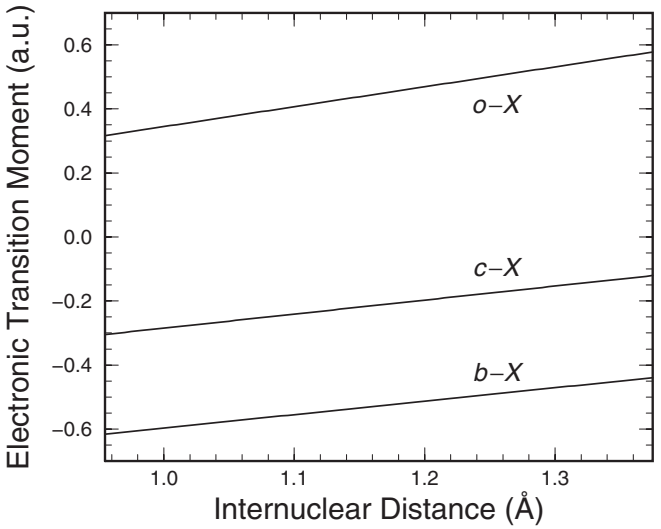

FIG. 2. Diabatic optical electronic transition moments used in the CC model (see text).

intensity-pattern-forming parameter determined through the fitting process is the GETM ratio

$$r = \frac{(M_{cX}/M_{bX})}{(M_{cX}/M_{bX})_{\text{opt.}}} = \frac{(M_{oX}/M_{bX})}{(M_{oX}/M_{bX})_{\text{opt.}}}. \tag{6}$$

IV. RESULTS AND DISCUSSION

A. Experimental GVOSs

The extremes of behavior for different vibrational bands of the $b\ ^1\Pi_u - X\ ^1\Sigma_g^+(v,0)$ system are illustrated in Fig. 3, where experimental GVOS patterns for the (2,0) and (5,0) bands are shown, together with room-temperature optical oscillator strengths ($K^2 = 0$), derived from the J-dependent results of Stark *et al.* [47,48]. Each GVOS pattern is consistent with the corresponding optical value. However, for all impact energies, there is a startling difference between the patterns of the two bands. Consistent with expectation for a well-behaved allowed electronic transition, in the case of the (2,0) band the GVOS decreases essentially monotonically as K^2 increases, by around an order of magnitude over the range of momentum transfer covered by the experiment. On the other hand, in the case of the (5,0) band, there is a near-zero minimum in the region $K^2 = 0.2$–0.4 a.u., before the GVOS rises again at higher K^2.

Measurements of the $^1\Pi_u \leftarrow X\ ^1\Sigma_g^+$ bands have been singled out here for a detailed appraisal of the $E_0 = 100$ eV spectrum. These cover the range 12.5–13.7 eV and terminate on the excited-state levels $b(0-13)$, $c(0-2)$, and $o(0-1)$. At this value of E_0, the contributions of forbidden transitions to the energy-loss spectrum may be neglected, and thus the respective GVOSs of the $^1\Pi_u$ X bands have all been determined individually, apart from b-$X(9,0)$ and o-$X(1,0)$, which are treated as an integrated pair. In order to emphasize the anomalous effects which are of most interest to this work,

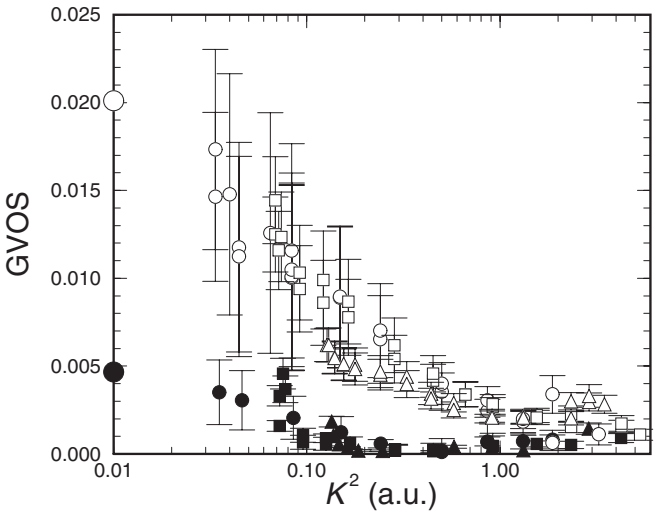

FIG. 3. Comparison of experimental GVOSs for b-$X(5,0)$ and b-$X(2,0)$ bands of N_2 (solid and open symbols, respectively). Circles: $E_0 = 100$ eV. Squares: $E_0 = 50$ eV. Triangles: $E_0 = 30$ eV. The optical oscillator strengths of Stark *et al.* [47], adjusted to room temperature [48], are also shown (large circles, plotted on the GVOS-axis for convenience).

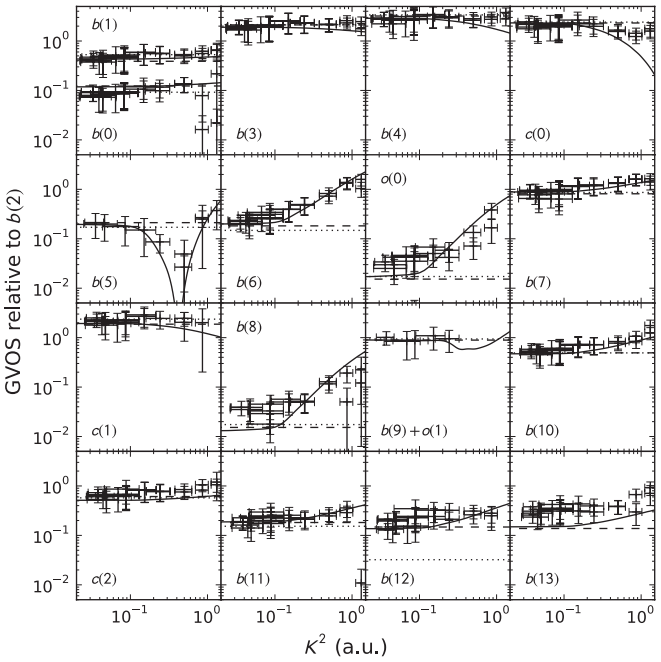

FIG. 4. Comparison between experimental ($E_0 = 100$ eV) and coupled-channel GVOSs for the $^1\Pi_u - X\ ^1\Sigma_g^+$ bands of N_2, with all quantities plotted relative to the modeled GVOS for b-$X(2,0)$. Error bars: Experimental values from present energy-loss spectra. Solid lines: Values computed using optimized CC model. Dashed lines: Optical oscillator strengths of Ref. [47] ($K^2 = 0$). Dotted lines: Near-optical GVOSs from Ref. [12]. Graphs are labeled according to the excited-state vibrational level, ignoring any overlapping triplet levels which are not expected to contribute significantly (see Sec. II).

henceforth all GVOS are described relative to that of the well-behaved b-$X(2,0)$ band, shown in Fig. 3.

In Fig. 4, the experimental GVOSs of the $^1\Pi_u \leftarrow X$ bands for $E_0 = 100$ eV and $K^2 < 1.5$ are plotted, normalized to the modeled GVOS for b-$X(2,0)$, which is described in Sec. IV B. Also plotted are the optical oscillator strengths of Stark *et al.* [47,48] and GVOSs derived from the electron energy-loss spectra of Geiger and Schröder [12]. The former results correspond definitively to $K^2 = 0$, and the kinematic conditions of the latter lead to $K^2 \simeq 4 \times 10^{-3}$ a.u., i.e., equivalent to near-optical conditions. The relative experimental vibrational band intensities in Fig. 4 display a wide range of patterns of variation with momentum transfer, inconsistent with the normal expectation of constancy for an isolated electronic transition. Nevertheless, in the limit of low K^2, overall there is excellent agreement with the optical and near-optical results of Refs. [47] and [12], respectively. The principal exception is for b-$X(12,0)$, where the result of Geiger and Schröder [12] is anomalously low, possibly due to incorrect partitioning [47] of the energy-loss cross section between adjacent bands in this region of the limited-resolution EELS spectrum of Ref. [12]. The optical measurements of Stark *et al.* [47] are rotationally resolved and thus do not suffer from such problems. Ignoring the b-$X(12,0)$ result of Ref. [12], the worst agreement in Fig. 4 occurs for b-$X(8,0)$, o-$X(0,0)$, and b-$X(13,0)$, with the present low-K^2 results somewhat higher than the optical values in each case. The b-$X(8,0)$ and o-$X(0,0)$ bands are by far the weakest studied, and are therefore expected to be more subject to error

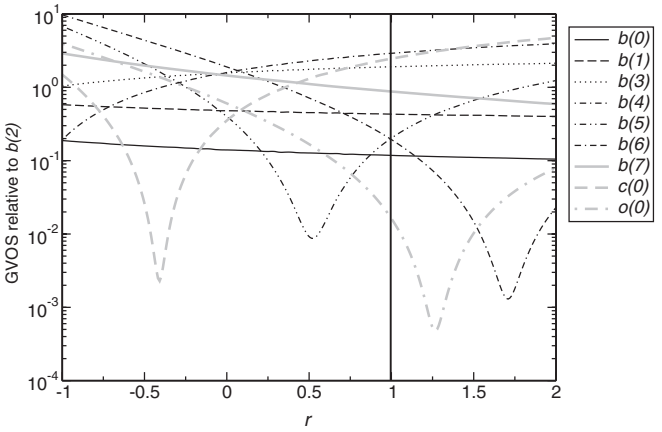

FIG. 5. Calculated GVOSs of selected $^1\Pi_u \leftarrow X$ bands, relative to b-$X(2,0)$, labeled according to the excited-state vibrational level. The independent variable r is scanned by modifying the GETMs of the Rydberg c and o states by a common factor. The vertical line ($r = 1$) corresponds to optical conditions.

in the spectral unfolding process, while the larger discrepancy for b-$X(13,0)$ may be caused by partitioning errors due to the limited spectral resolution in the current experiment.

B. Coupled-channel GVOSs

As described in Sec. III B, only the electronic transition moments from the previous CC model [35,36] are modified for the current application, in order to extend to the case of finite momentum transfer, thereby forming GETMs. The Rydberg-to-valence GETM ratio r, defined by Eq. (6), is the key parameter of the new model, together with a single overall R-independent scaling factor, needed to reproduce the experimental GVOSs.

Figure 5 shows GVOSs calculated for a range of r and a selection of $^1\Pi_u \leftarrow X$ bands, plotted relative to the CC GVOS of b-$X(2,0)$. A value of $r = 1$ corresponds to the previous CC model [35,36], relating specifically to optical conditions. As for the experimental results in Sec. IV A, a normalization was adopted relative to b-$X(2,0)$ because this excited level is of essentially pure b-state valence electronic character, and removing this dependence serves to further emphasize the occurrence of quantum interference between the Rydberg and valence generalized transition amplitudes.

Several of the bands in Fig. 5 have rotationally dependent oscillator strengths. In particular, the strength of o-$X(0,0)$ increases by an order of magnitude between $J = 1$ and 22, as does b-$X(5,0)$ between $J = 1$ and 20 [47]. In order to calculate strengths that are comparable to the band-averaged measurements, separate model line strengths are calculated for the $Q(4)$, $Q(6)$, $Q(8)$, $Q(10)$, and $Q(12)$ transitions. Averaging these gives an oscillator strength that is directly comparable with the experiment. For this averaging, a Boltzmann distribution of ground-state levels is adopted, assuming a temperature of 300 K. The contributions of P- and R-branch transitions are neglected in these calculations, even though Stark *et al.* [47] have observed significant differences in the effective oscillator strengths for these branches. This occurs because of a quantum-interference effect involving nearby,

rotationally perturbing electronic states of $^1\Sigma_u^+$ symmetry [1], and commonly leads to an equal and opposite modification of the P- and R-branch line strengths, relative to the Q-branch line of the same excited-state J value. A preliminary extension was made to the CC model [49], explicitly including the b' and c' $^1\Sigma_u^+$ states, as well as rotational coupling to the $^1\Pi_u$ manifold. The resultant P- and R-branch oscillator strengths were broadly consistent with the observations of Stark *et al.* [47], as well as the behavior of the $^1\Sigma_u^+$ levels observed in the present electron energy-loss spectra. However, for the purposes of modeling the bands depicted in Fig. 4, the extended model is not required because, fortuitously, when averaged, the perturbed P- and R-branch oscillator strengths are equivalent, within experimental error, to that of the Q branch.

As shown in Fig. 5, the modeled relative GVOSs of transitions to b(0–4) and b(7) show only a gradual variation with r, whereas those to b(5), b(6), c(0), and o(0) display deep minima where the b- and c-state generalized transition amplitudes interfere destructively. It is not expected that the GETM of either state, and hence r, will change sign as K^2 is increased (i.e., $r > 0$), so the interference minimum for c-X(0,0) is unlikely to be observed experimentally. Similarly, the expectation of a more rapid falloff for Rydberg-state GETMs than for valence states (i.e., $r < 1$) [6] for increasing momentum transfer makes unlikely the observation of the minima for b-X(6,0) and o-X(0,0). However, in agreement with the predictions of the CC model in Fig. 5, a minimum is observed in the b-X(5,0) experimental GVOS plotted in Fig. 3, for all impact energies. Similarly, the presence, and sense, of the variations in the other observed relative GVOSs in Fig. 4 are in qualitative agreement with Fig. 5, supporting the notion of a correlation between $1 - r$ and K^2, as suggested for the case of transitions to the valence-Rydberg-mixed $^3\Sigma_u^-$ and $^3\Pi_u$ states of O_2 [6].

C. Optimized GETMs

There is sufficient experimental information here to attempt a quantitative assessment of the variation of model GETMs with increasing momentum transfer. The M_{bX}, M_{cX}, and M_{oX} diabatic electronic transition moments of Haverd *et al.* [36] were adopted as GETMs corresponding to $K^2 = 0$. These were then scaled to best fit the observed GVOSs of b-X(2,0) and b-X(5,0) for a range of K^2, initially for the case $E_0 = 100$ eV. The M_{cX} and M_{oX} GETMs were scaled by a common factor during the optimization, as implied by Eq. (6).

The isolated b(2) level was selected as a constraint for the fitting process because it leads to a reliable measure of the M_{bX} GETM, independent of the Rydberg states, whereas the pronounced interference observed for the b(5) level provides a severe constraint on the $^1\Pi_u \leftarrow X$ Rydberg GETMs. The optimized scaling factors obtained in this fashion were then interpolated smoothly in order to reduce the effect of experimental scatter. The resulting smoothed $E_0 = 100$ eV diabatic GETMs, plotted relative to the optical case in Fig. 6 (solid curves), are seen to decrease monotonically with increasing K^2, and more quickly for the Rydberg states, as found previously in the case of O_2 [6]. The smoothness of the optimized GETMs is deceptive: an uncertainty of $\sim\pm0.1$ is estimated for the scaling factors plotted in Fig. 6. arising from

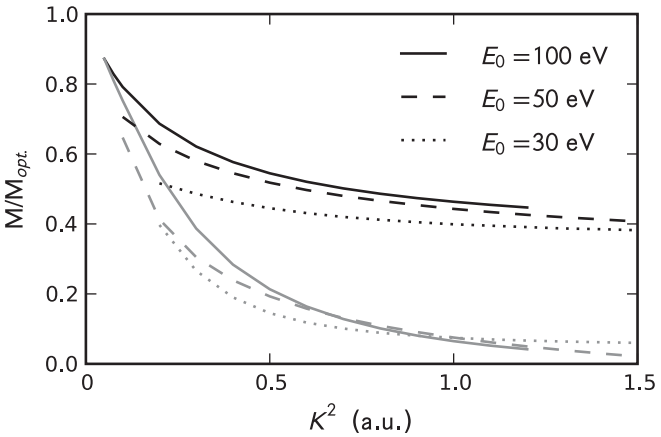

FIG. 6. Scaling of optical transition moments necessary to reproduce the observed GVOSs of b-X(2,0) and b-X(5,0) bands. For the three cases, $E_0 = 100$, 50, and 30 eV, the scaling of M_{bX} relative to the optical case is plotted in black, and the common scaling of M_{cX} and M_{oX} is plotted in gray.

experimental noise, an imperfect division of spectral intensity between bands, and the neglect of the $^1\Sigma_u^+$ states and associated rotational perturbations.

Figure 4 shows a high level of agreement between the experimental and modeled $E_0 = 100$ eV GVOSs, which were computed using the optimized GETMs described above. Particularly encouraging is the large and correctly-modeled variation in relative GVOS observed for b-X(6,0) and b-X(8,0) [50], which can only be effected by quantum interference induced by a mixed electronic character. Furthermore, the calculated, and observed, relative GVOSs of o(0)-X(0) [50] are seen to increase with K^2 despite the rapidly decreasing o-X GETM, also indicating the presence of quantum interference. None of these effects were referenced during the GETM optimization procedure, which used only the b-X(2,0) and b-X(5,0) experimental results. Thus, the excellent agreement between experiment and theory for nearly all bands in Fig. 4 is a powerful validation of the CC approach and the GETM concept. Only in the case of the c-X(0,0) band is there a significant model-experiment variation discrepancy, the modeled GVOS decreasing faster at high K^2. While it is possible that further improvements to the CC model might be required to resolve this discrepancy, its most likely explanation is uncertainty in the unfolding of the c-X(0,0) contribution from the adjacent, very strong c'-X(0,0) contribution to the EEL spectrum.

Optimized GETMs were also determined from the GVOS measurements for $E_0 = 50$ and 30 eV, and a similar good level of agreement between the corresponding GVOSs and experiment was found as for the $E_0 = 100$ eV case in Fig. 4. The functional decreases with increasing K^2 of these optimized GETM scaling factors are also plotted in Fig. 6 (dashed and dotted curves, respectively). In all cases the GETMs of the Rydberg states decrease faster than for the valence state, and the lower intensities observed for decreasing E_0 lead to smaller model GETMs. The latter trend, also observed in the case of O_2 [6], points to an inapplicability of the first Born approximation, which would require that

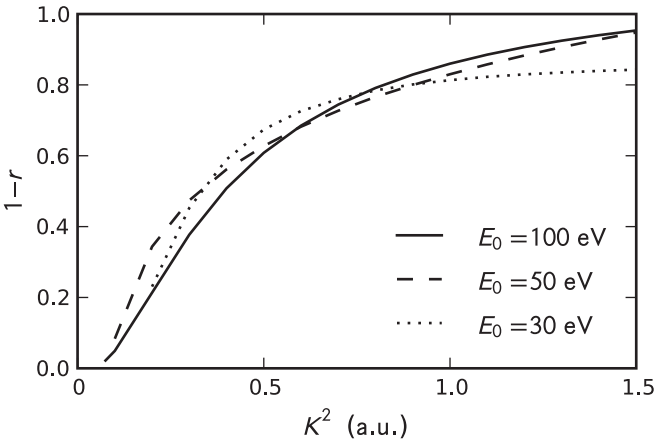

FIG. 7. Relationship between $1 - r$ and K^2 for the scattering of $E_0 = 100$, 50, and 30 eV electrons. Here, r, defined by Eq. (6), is the ratio of Rydberg- to valence-state GETMs, relative to optical conditions.

the GVOS be independent of all scattering parameters apart from the momentum transfer. It remains true, however, that the GVOS will approach the optical oscillator strength in the limit of small K^2 for all cases [6].

Finally, Fig. 7 shows the ratio of the optimized scaling of Rydberg- to valence-state GETMs, derived from the experimental results, plotted as $1 - r$ versus K^2. The estimated uncertainty in r is typically ± 0.14. By definition, $r = 1$ when $K^2 = 0$, i.e., under optical conditions. That the smoothed experimental curves deviate slightly from an intercept at the origin of Fig. 7 is explained by the experimental uncertainties. The three curves in Fig. 7 exhibit similar behaviors, with $1 - r$ increasing rapidly with K^2 before leveling off, the rate of increase being somewhat larger for the lower impact energies. This type of behavior is very similar to that determined from mixed valence-Rydberg bands observed in the O_2 energy-loss spectra of [6], but with a slightly lower rate of increase. The key conclusion from Fig. 7 is that the Rydberg GETMs decrease much faster than the valence GETM as the momentum transfer increases away from optical conditions. This can be understood by considering the diffuse nature of the Rydberg orbitals and the correspondingly increased sensitivity to the influence of the impacting electron [6].

V. SUMMARY AND CONCLUSIONS

Building on the work of [6], the usefulness of the GETM concept in concert with CC Schrödinger-equation calculations has been demonstrated quantitatively for the study of anomalous vibrational intensities in the EEL spectra of coupled electronic states of N_2. Spectra covering a large number of $^1\Pi_u \leftarrow X$ bands have been measured for a range of impact energies and scattering angles, and reduced to individual generalized oscillator strengths for each band. These data have been reproduced for a range of K^2 covering two orders-of-magnitude by a CC model treating the Rydberg-valence interactions in the $^1\Pi_u$ manifold. Only two independent momentum-transfer-dependent model parameters were varied in order to achieve a global fit to the observations. The critical parameter controlling the quantum-interference effects which lead to anomalous relative band intensities is the ratio r of the Rydberg- and valence-state generalized transition moments. The demonstrated correlation between $1 - r$ and K^2 leads to the ability to control these interference effects, and thus the relative vibrational intensities in EEL spectra, simply by changing the experimental scattering conditions. This interesting possibility contrasts with the case of optical spectra, where the corresponding interference effects are controlled by the fixed molecular electronic transition moments which are out of the control of the experimentalist. Remarkably, in the case of N_2, the b-$X(5,0)$ transition in the EEL spectra can be tuned almost out of existence by ensuring that K^2 is in the region of 0.3 a.u., leading to total destructive interference between the valence and Rydberg generalized transition amplitiudes.

ACKNOWLEDGMENTS

The theoretical component of this work was supported by the Australian Research Council Discovery Program, through Grants No. DP0558962 and No. DP0773050. Experimental aspects of this work were performed at the Jet Propulsion Laboratory, California Institute of Technology, under a contract with the National Aeronautics and Space Administration (NASA), and at the California State University, Fullerton. Financial support through NASA's Planetary Atmospheres and Outer Planets research programs, and the National Science Foundation (Grants No. NSF-PHY-RUI-0653452 and No. NSF-AGS-0938223) is gratefully acknowledged.

[1] H. Lefebvre-Brion and R. W. Field, *The Spectra and Dynamics of Diatomic Molecules* (Elsevier, Amsterdam, 2004), pp. 378–406.
[2] H. A. Bethe, Ann. Phys. (Leipzig) **397**, 325 (1930).
[3] E. N. Lassettre, A. Skerbele, and M. A. Dillon, J. Chem. Phys. **50**, 1829 (1969).
[4] M. Shugard and A. U. Hazi, Phys. Rev. A **12**, 1895 (1975).
[5] M. Dillon, M. Kimura, R. J. Buenker, G. Hirsch, Y. Li, and L. Chantranupong, J. Chem. Phys. **102**, 1561 (1995).
[6] B. R. Lewis, J. P. England, S. T. Gibson, M. J. Brunger, and M. Allan, Phys. Rev. A **63**, 022707 (2001).
[7] H. Lefebvre-Brion, Can. J. Phys. **47**, 541 (1969).
[8] K. Dressler, Can. J. Phys. **47**, 547 (1969).
[9] P. K. Carroll and C. P. Collins, Can. J. Phys. **47**, 563 (1969).
[10] M. A. Khakoo, C. P. Malone, P. V. Johnson, B. R. Lewis, R. Laher, S. Wang, V. Swaminathan, D. Nuyujukian, and I. Kanik, Phys. Rev. A **77**, 012704 (2008).
[11] G. Joyez, R. I. Hall, J. Reinhardt, and J. Mazeau, J. Electron Spectrosc. Relat. Phenom. **2**, 183 (1973).
[12] J. Geiger and B. Schröder, J. Chem. Phys. **50**, 7 (1969).
[13] M. A. Khakoo, P. V. Johnson, I. Ozkay, P. Yan, S. Trajmar, and I. Kanik, Phys. Rev. A **71**, 062703 (2005).

[14] M. A. Khakoo, K. Keane, C. Campbell, N. Guzman, and K. Hazlett, J. Phys. B **40**, 3601 (2007).
[15] M. Hughes, K. E. James, J. G. Childers, and M. A. Khakoo, Meas. Sci. Technol. **14**, 841 (2003).
[16] S. Trajmar, D. F. Register, D. C. Cartwright, and G. Csanak, J. Phys. B **25**, 4889 (1992).
[17] M. Hoshino, H. Kato, H. Tanaka, I. Bray, D. V. Fursa, S. J. Buckman, O. Ingólfsson, and M. J. Brunger, J. Phys. B **42**, 145202 (2009).
[18] R. Ward, D. Cubric, N. Bowring, G. C. King, F. H. Read, D. V. Fursa, I. Bray, O. Zatsarinny, and K. Bartschat, J. Phys. B **44**, 045209 (2011).
[19] C. P. Malone, P. V. Johnson, I. Kanik, B. Ajdari, and M. A. Khakoo, Phys. Rev. A **79**, 032704 (2009).
[20] C. P. Malone, P. V. Johnson, I. Kanik, B. Ajdari, S. S. Rahman, S. S. Bata, A. Emigh, and M. A. Khakoo, Phys. Rev. A **79**, 032705 (2009).
[21] J. Muse, H. Silva, M. C. A. Lopes, and M. A. Khakoo, J. Phys. B **41**, 7 (2008).
[22] I. Linert and M. Zubek, J. Phys. B **42**, 085203 (2009).
[23] S. K. Srivastava, A. Chutjian, and S. Trajmar, J. Chem. Phys. **64**, 1340 (1976).
[24] S. Trajmar, D. F. Register, and A. Chutjian, Phys. Rep. **97**, 221 (1983).
[25] T. W. Shyn and G. R. Carignan, Phys. Rev. A **22**, 923 (1980).
[26] J. C. Nickel, C. Mott, I. Kanik, and D. C. McCollum, J. Phys. B **21**, 1867 (1988).
[27] M. Gote and H. Ehrhardt, J. Phys. B **28**, 3957 (1995).
[28] E. F. van Dishoeck, M. C. van Hemert, A. C. Allison, and A. Dalgarno, J. Chem. Phys. **81**, 5709 (1984).
[29] L. Torop, D. G. McCoy, A. J. Blake, J. Wang, and T. Scholz, J. Quant. Spectrosc. Radiat. Transfer **38**, 9 (1987).
[30] W.-Ü. L. Tchang-Brillet, P. S. Julienne, J.-M. Robbe, C. Letzelter, and F. Rostas, J. Chem. Phys. **96**, 6735 (1992).
[31] B. R. Lewis, S. S. Banerjee, and S. T. Gibson, J. Chem. Phys. **102**, 6631 (1995).
[32] J. Lacoursière, S. A. Meyer, G. W. Faris, T. G. Slanger, B. R. Lewis, and S. T. Gibson, J. Chem. Phys. **110**, 1949 (1999).
[33] B. R. Lewis, S. T. Gibson, F. T. Hawes, and L. W. Torop, Phys. Chem. Earth C **26**, 519 (2001).
[34] B. R. Lewis, S. T. Gibson, J. S. Morrill, and M. L. Ginter, J. Chem. Phys. **111**, 186 (1999).
[35] B. R. Lewis, S. T. Gibson, W. Zhang, H. Lefebvre-Brion, and J.-M. Robbe, J. Chem. Phys. **122**, 144302 (2005).
[36] V. E. Haverd, B. R. Lewis, S. T. Gibson, and G. Stark, J. Chem. Phys. **123**, 214304 (2005).
[37] B. R. Lewis, A. N. Heays, S. T. Gibson, H. Lefebvre-Brion, and R. Lefebvre, J. Chem. Phys. **129**, 164306 (2008).
[38] B. R. Lewis, K. G. H. Baldwin, A. N. Heays, S. T. Gibson, J. P. Sprengers, W. Ubachs, and M. Fujitake, J. Chem. Phys. **129**, 204303 (2008).
[39] M.-C. Liang, G. A. Blake, B. R. Lewis, and Y. L. Yung, Proc. Nat. Acad. Sci. USA **104**, 21 (2007).
[40] M.-C. Liang, A. N. Heays, B. R. Lewis, S. T. Gibson, and Y. L. Yung, Astrophys. J. **664**, L115 (2007).
[41] X. Liu, A. N. Heays, D. E. Shemansky, B. R. Lewis, and P. D. Feldman, J. Geophys. Res. **114**, D07304 (2009).
[42] M. H. Stevens *et al.*, J. Geophys. Res. **116**, A05304 (2011).
[43] P. Lavvas, M. Galand, R. V. Yelle, A. N. Heays, B. R. Lewis, G. R. Lewis, and A. J. Coates, Icarus **213**, 233 (2011).
[44] C. J. Hansen *et al.*, Geophys. Res. Lett. **38**, L11202 (2011).
[45] D. Stahel, M. Leoni, and K. Dressler, J. Chem. Phys. **79**, 2541 (1983).
[46] D. Spelsberg and W. Meyer, J. Chem. Phys. **115**, 6438 (2001).
[47] G. Stark, K. P. Huber, K. Yoshino, P. L. Smith, and K. Ito, J. Chem. Phys. **123**, 214303 (2005); G. Stark, B. R. Lewis, A. N. Heays, K. Yoshino, P. L. Smith, and K. Ito, *ibid.* **128**, 114302 (2008).
[48] For the present purposes, the Q-branch oscillator strengths of Ref. [47] for an effective $J = 9$ were taken to approximate room-temperature experimental values.
[49] A. N. Heays, Ph.D. thesis, The Australian National University, 2011 (unpublished).
[50] The agreement between the experimental and modeled GVOS variations for the b-$X(8,0)$ and o-$X(0,0)$ bands may be even better than indicated in Fig. 4 if allowance is made for the possible problems in unfolding the low-K^2 GVOSs for these very weak bands, as discussed in Sec. IV A.